WHC-SA-1010-FP

Comparison of Reinforced-Concrete Models for Use in the Analysis of Extreme Loads

Prepared for the U.S. Department of Energy
Office of Environmental Restoration and Waste Management

Westinghouse Hanford Company Richland, Washington

Hanford Operations and Engineering Contractor for the
U.S. Department of Energy under Contract DE-AC06-87RL10930

Approved for Public Release

WHC-SA--1010

DE91 010108

Comparison of Reinforced-Concrete Models for Use in the Analysis of Extreme Loads

A. D. Dyrness
J. L. Julyk

Date Published
March 1991

To be presented at
1991 ASME Pressure Vessel
and Piping Conference
San Diego, California
June 23-27, 1991

Prepared for the U.S. Department of Energy
Office of Environmental Restoration and Waste Management

Westinghouse
Hanford Company

P.O. Box 1970
Richland, Washington 99352

Hanford Operations and Engineering Contractor for the
U.S. Department of Energy under Contract DE-AC06-87RL10930

ABSTRACT

Extreme load analyses of concrete structures rely on the concrete constitutive model and the solution procedure to preserve solution accuracy throughout the analysis as well as to assure numerical stability in highly inelastic regimes. The application of existing finite-element software to extreme load analysis of reinforced-concrete structures is the focus of this paper. Two reinforced-concrete constitutive models, associated with commercially available software, are compared. One is an internal material model contained in the general purpose finite-element program, ABAQUS[c]. The other (ANACAP-U[d]) is a concrete analysis package that provides a reinforced-concrete material subroutine (UMAT90[e]) linked to ABAQUS. Solution accuracy is quantified by comparing the analysis predicted 'load-versus-displacement' curves with experimental results for a two-way reinforced-concrete slab with pinned supports and a concentrated load at its center. Although other investigators have had reasonable success correlating to experimental results, the range of the correlations has not challenged the convergence of the constitutive models under excessive tensile strain conditions. Parametric analyses documented herein assess the sensitivity of convergence to various parameters. These parameters include the application of the large displacement theory, solution procedures, strain hardening effects, rebar plasticity, and element type. The comparisons reported herein provide a basis for selecting a commercially available, reinforced-concrete material model and solution procedure for application to extreme load analyses.

---

[a] ADVENT Engineering Services, Inc.
[b] Westinghouse Hanford Company.
[c] ABAQUS is a trademark of Hibbitt, Karlsson & Sorensen, Inc.
[d] ANACAP-U is a trademark of Anatech Research Corp.
[e] UMAT90 is a trademark of Anatech Research Corp.

INTRODUCTION

Reinforced concrete in combination with a steel liner has had a wide application to confinement structures containing hazardous material. The double-shell waste storage tanks at the U.S. Department of Energy's Hanford Site use this type of construction. The performance goals defined for these tanks typically require these structures to be analyzed for low probability, beyond-design-basis loads. The response of reinforced-concrete structures subjected to extreme loads is often characterized by gross exceedance of the material elastic limit without loss of integrity. In such extreme load scenarios, failure may be defined by structural instabilities at loads well beyond those associated with material strength-based allowables defined by conventional codes and standards. The use of finite-element methods in predicting such failures requires a reinforced-concrete constitutive model that accounts for nonlinear post-cracking behavior. Most of the existing literature on modeling the nonlinear behavior of reinforced concrete focuses on improving the accuracy or numerical stability of the constitutive model itself. The comparisons presented herein address both the numerical stability associated with post-cracking tensile strains and solution accuracy of two existing constitutive models.

BACKGROUND

Following the 1978 Three Mile Island accident, several research programs were initiated to develop a better reinforced-concrete constitutive model for use in providing more reliable predictions of the response of steel-lined reactor containment structures subject to accident conditions. Hanford Site steel-lined waste tank structures, analysed for worse-case-accident internal-pressure loading, behaves as a tension structure with response regimes and failure mechanisms similar to those of reactor containment.

The steel liner and concrete reinforcement in the Hanford Site double-shell waste storage tanks represent a parallel internal-pressure load-carrying capability. Modeling of this construction to address tension behavior should allow for results indicative of stable structural behavior, even with significant tensile strains in the reinforced-concrete backing. The onset of instability, if modelled correctly, should be characterized by excessive liner tensile strains as the ultimate tensile strength is approached. Therefore, an accurate solution requires that the concrete constitutive model and solution algorithm maintain numerical stability in the tensile regime.

The modeling of complex tensile behavior of reinforced concrete in finite-element analyses has been known to introduce numerical instabilities (Cristfield 1984; Cristfield 1986; and Gonzales-Vidosa et al. 1988). The instabilities are associated, in general, with the application of tensile strain softening (tension softening in plain concrete or tension stiffening in reinforced concrete) in conjunction with classical local continuum theory. Instability during solution iterations can manifest itself in a number of ways. The introduction of alternate (unstable) equilibrium states can result from the modeling of tension stiffening (Crisfield 1986). Parallel cracks that occur within an element with little or no shear retention can lead to small pivots, thereby causing numerical instabilities (Gonzales-Vidosa 1988). The numerical solution procedure itself plays a significant role in determining the stability of the cracked concrete's structural response. Residual forces caused by crack initiation can be on the same order as the applied loads, making it impossible to attain equilibrium convergence. Recognizing that the primary interest of such analyses is in the global response; a balance between stability and the accuracy of the reinforced-concrete material characterization is required.

Tensile stress-strain data for reinforced concrete is scarce in the literature. The shape of the tensile stress-strain diagram is well known but there is a wide disparity in the literature on the control points. It is an accepted practice to use a linear stress-strain relationship with a slope equal to the compressive tangent modulus until the fracture stress is reached, as shown in Figure 1. The fracture stress of concrete generally ranges from 5 to 15 percent of its compressive strength. Beyond the fracture strain, the corresponding stress monotonically reduces to zero over a finite range of strain. This 'tension stiffening' phenomenon is evidence of the transfer of load from the concrete to the rebar over a finite range of strain. The strain at which the concrete tensile stress reaches zero ranges in the literature from 2 to 20 times the fracture strain (Cope 1984; Schnobrich 1990). The appropriate value is a function of the percentage of reinforcement and possibly mesh size. A value of 2 would correspond to plain or lightly reinforced concrete while the value of 20 would correspond to heavily reinforced concrete. In addition to tensile load transfer, shear loads are transferred across cracks over a finite range of strain. This 'shear retention' phenomena is evidence of shear transfer as a result of aggregate interlock within rough cracks and the dowel action of reinforcing bars.

MODEL DESCRIPTION

The two constitutive models, although both using the 'smeared crack' approach, have significant differences between them. In brief, UMAT90 (ANATECH 1990a; ANATECH 1990b) model (MAT1) requires Young's modulus, Poisson's ratio, the compressive strength, and the tensile fracture strain for static analyses. All other structural properties are calculated internally using an extensive database of concrete material properties. The tensile strength is calculated from the fracture strain and Young's modulus. The post-cracking tensile stress-strain diagram is represented by a linear curve from the fracture point to zero stress at a strain equal to approximately two times the fracture strain, as shown in Figure 1. This tensile behavior basically accounts for tension softening of plain concrete, a physical property of the material, which is considered to be independent of the mesh size and rebar quantities (ANATECH 1990a). Tension stiffening of the reinforced concrete, with the attendant potential for mesh sensitivity, is not addressed. MAT1 accounts for shear transfer across cracks via a 'rough crack' model that is independent of reinforcement quantity or aggregate size. This model reduces the shear modulus of the concrete as a function of tensile strain. Once a crack is formed, the shear modulus drops to 40 percent of its uncracked value. It is further reduced inversely proportional to the tensile strain beyond crack initiation. The triaxial yield surface, which is important for concrete under significant compressive or highly confining loads, is computed internally.

The ABAQUS (Jofriet 1971) concrete model (MAT2) input requirement includes Young's modulus, Poisson's ratio, the compressive stress-strain diagram, parameters that address the tensile behavior, and parameters that address the shape of the triaxial yield surface. The compressive stress-strain behavior used here in MAT2 is bilinear with a yield strength of 20.7 MPa (3,000 lbf/in^2) and an ultimate strength of 37.95 MPa (5,500 lbf/in^2) at 1.5 percent plastic strain. The direction of the first crack at each integration point corresponds to that of the maximum principal strain. Subsequent cracks at such points are formed only in orthogonal directions. The crack directions at each integration point are independent. MAT2 requires that the post-cracking tensile stress-strain diagram be input by the user and is specified in this work, as shown in Figure 1. Shear transfer across cracks is normally described in MAT2 by a linear reduction in the uncracked shear modulus to zero at a user-specified strain. In this work the shear modulus is relatively unimportant and is assumed constant in the MAT2 specification. The fracture strain is computed based on Young's modulus; the compressive strength, and the tensile-to-compressive strength ratio are required as input by the user. The base case model with MAT2 uses the following constitutive parameters:

- Ratio of biaxial compressive to uniaxial compressive strength, 1.16 (default) (Jofriet 1971)
- Ratio of uniaxial tensile to uniaxial compressive strength, 0.086 (given) (Gilbert and Warner 1978)

- Ratio of principal plastic strain magnitude in biaxial compression to the plastic strain under uniaxial compression, 1.28 (default) (Jofriet 1971)

- Ratio of tensile principal stress under plane stress conditions when the other principal stress is at the ultimate compressive strength to the uniaxial tensile cracking stress, 0.333 (default) (Jofriet 1971).

The well known experimental data from Jofriet and McNeice (1971) is used as an experimental benchmark because of the relatively simple geometry. The McNeice slab depicted in Figure 2 is a two-way reinforced-concrete slab with overall dimensions of 91.44 by 91.44 by 4.45 cm (HKS 1989b). The following material data was given (Gilbert and Warner 1978):

Modulus of elasticity for concrete (4.15E6 lbf/in^2)	= 2.86 E4 MPa
Modulus of elasticity for rebar (29.0E6 lbf/in^2)	= 2.00 E5 MPa
Concrete compressive strength (5,500 lbf/in^2)	= 37.95 MPa
Rebar yield strength (50,000 lbf/in^2)	= 3.45 E2 MPa
Poisson's ratio	= 0.15
Rebar/concrete ratio (each way)	= 0.0085
Rebar location from top of slab (1.31 in.).	= 3.33 cm

The mesh takes advantage of the double symmetry and is shown in Figure 3 for the shell element model and the solid element model. The load is applied at the center of the slab. In the actual experiment, the displacements were measured 7.62 cm (3 in.) from the load point. The displacements reported here are taken at the point of load application.

DISCUSSION

The parametric cases presented here are summarized in Table 1. Case 1 represents MAT2 and uses eight-node shell elements with four integration points (IP) and nine section points (SP) through the thickness. The rebar is treated as elastic-perfectly plastic (EPP). It also employs the modified Riks solution algorithm, which treats the applied load as part of the solution instead of an applied boundary condition. This algorithm is designed for nonlinear problems involving structural instabilities and is generally applicable to static ultimate capacity analyses. The ultimate load is defined by the load at the onset of structural instability. One disadvantage of the Riks algorithm in the current 4.8 version of ABAQUS is that restarts are not available from this procedure. Case 2 is identical to Case 1, except that the normal Newton solution algorithm is used with the equilibrium convergence criteria removed by implementing the NOSTOP option. This is the standard solution technique used when invoking the MAT1 constitutive model; it requires the analyst to use the force and displacement residuals and the stress result trends in determining the solution validity. It is used with MAT2 for comparison. Case 3 is also identical to Case 1, except that the large deflection theory is employed. The large deflection theory is often an important parameter in the evaluation of structures subjected to beyond-design-basis loads.

The McNeice central load-versus-displacement data are plotted in Figure 4 where they are shown to agree with the results of Cases 1, 2, and 3. The difference between the Riks method and the use of the NOSTOP option is hardly noticeable. Therefore, the careful use of the NOSTOP option can result in reliable predictions for design-basis loading. The application of the large displacement theory, as expected, has no impact on the solution accuracy within the range of the McNeice data.

Cases 4 through 8 are derivatives of Case 1 and are exercised to determine the sensitivity of the numerical stability to the material definition. Case 4 requires the rebar to remain totally elastic (TE). Although this treatment is unrealistic, it does indicate the sensitivity of the numerical stability to rebar plasticity. Case 5 artificially increases the concrete strength by specifying excessive strain hardening in the compressive stress-strain diagram (MAT2/SH) while the rebar treatment remains EPP. Case 6 artificially increases the rebar strength by specifying excessive elastic-plastic strain hardening (EPSH) in the steel stress-strain diagram while the concrete remains identical to Case 1. Case 7 attempts to add stability to the solution of Case 1 by adding a soft elastic liner in parallel with the concrete elements, while leaving the concrete and rebar material specifications the same as those in Case 1. Case 8 is identical to Case 7, except that the NOSTOP option in the solution procedure is employed.

The totally elastic treatment of the rebar in Case 4 resulted in a solution that diverged at a smaller central displacement than even the base case. A possible reason for this, while the elastic rebar provides for a greater strength, the convergence criteria of the Riks method was not increased. To do so would reduce the solution accuracy in the early stages of the solution. Although the solution diverged at 6.6 cm (2.6 in.) deflection, as shown in Table 1, the load was roughly four times the ultimate load predicted by Case 1. Increasing the concrete strength with artificial strain hardening in Case 5 significantly extended the solution stability. Numerical instability is generally associated with excessive tensile strains, and in the MAT2 model the tensile strength is proportional to the ultimate compressive strength, which implicitly makes for a more stable solution. It is apparent that the monotonic concrete compressive stress-strain behavior does not significantly affect the solution stability. Similar to the totally elastic rebar representation, rebar with excessive strain hardening in Case 6 results in premature numerical instability aggravated by the tight convergence criteria used with the Riks solution method. Although the maximum displacement was only 12.4 cm (4.9 in.), the load at instability was 51.62 kN (11,600 lb). The convergence criteria requires that the unbalanced forces be less than 178 N (40 lb). The addition of a soft elastic liner in Case 7 does not add to the solution stability. The instability is apparently associated with force imbalances during the cracking of the concrete elements and not with negative eigenvalues that can be

developed in the global stiffness matrix. The same ultimate load of 21.36 kN (4,800 lb) predicted by Case 7 is also predicted by Case 1. The addition of the NOSTOP option in Case 8 has no significant effect on the solution. The ultimate load of 21.36 kN (4,800 lb) predicted by Case 1 and 7 is replicated in Case 8.

Case 9 is the base case for the MAT1 model. It uses the NOSTOP option of the standard solution procedure. The use of the Riks solution procedure and MAT1 are mutually exclusive. The concrete material properties are specified to be consistent with those for Case 1. UMAT90 is implemented via a user-defined material subroutine for which ABAQUS requires the specification of the transverse shear stiffness for shell elements. The ABAQUS element formulation treats this stiffness elastically, even in a cracking element. As long as the element is thin with respect to its unsupported length, this approximation will have no significant impact on the solution. A reasonable value was used to avoid singularities. This model also compares reasonably well with the McNeice data is shown in Figure 4 with a slightly conservative prediction of the slab collapse load. This behavior is typical of constitutive models that do not apply tension stiffening. The seemingly better agreement provided by the MAT2 model is somewhat misleading, in that the solution depends on the specified tension-stiffening parameter, which usually is not known a priori.

Cases 10 and 11 are MAT1 analogies to Cases 4 and 7, respectively. Case 10 employs a totally elastic rebar representation. Case 11 includes a soft elastic liner in parallel with the concrete shell elements. Both the totally elastic treatment of the rebar and the addition of the soft elastic liner provided added stability to the MAT1 base case. Although this artificial treatment of the McNeice slab is not needed to predict its ultimate capacity, Cases 10 and 11 demonstrate that finite-element models using the MAT1 constitutive model can apply heuristic tactics to predict ultimate capacities of structures that are more susceptible to instability.

Case 12 is the MAT1 analogy to Case 3, where the large displacement option is implemented. The implementation of large displacement makes essentially no difference at the small displacements reported by McNeice for either constitutive model. Unlike Case 3, the application of the large displacement theory does not significantly affect the numerical stability of the MAT1 model. Excessive tensile strains are realized in Case 12, as reflected in the large slab displacements illustrated in Figure 5. There is a significant difference in the ultimate capacity, however. The application of the large displacement option increases the predicted ultimate load. The MAT2 model not only shows an increase in the ultimate load, but it also causes premature numerical divergence when used with the Riks algorithm.

Case 13 is identical to Case 1, except that the number of section points through the thickness is reduced from nine to three. This implicitly increased the bending stiffness. Cases 14 and 15 employ eight-node, solid elements with eight integration points. Case 14 uses the MAT2 constitutive model and the Riks solution algorithm. Case 15 is identical to Case 14 except that it applies the NOSTOP option of the ABAQUS standard solution procedure. The McNeice data end at a deflection of 0.81 cm (0.32 in.). The ultimate load is not known with certainty. It is clear from Figure 6 that the reduction in the number of section points through the thickness in Case 13 artificially stiffens the slab and tends to overpredict the ultimate load. Case 15, with its eight-node solid elements with the MAT2 material characterization shows an overestimation of the slab stiffness as well. This overestimation is caused in part by the use of the lower order elements whose bending stiffness is implicitly larger than the higher order 20-node solid elements. Also, Case 15 is an example of the over specification of tension stiffening. In this particular mesh, two thirds of the elements do not contain reinforcement, yet tension stiffening is specified for all the elements. Better results may be obtained by specifying lower values of tension stiffening for the plain concrete elements, at the cost of reduced numerical stability. Although it is not reliable, it is interesting to note that the ultimate load predicted by the aborted (Case 15) solution is not far from the ultimate load indicated by the McNeice data. This solid element solution was made available only through the use of the NOSTOP option. The Riks solution used in Case 14 diverges early into the solution, far short of the ultimate load. There are a number of unreinforced elements; thus satisfying the convergence criteria is even more difficult for the Riks algorithm.

Cases 16 and 17 are the MAT1 analogy to Cases 13 and 15, respectively. The reduced through-thickness integration applied in Case 16 shows a significant increase in the slab stiffness over the more refined integration included in the MAT1 base case. Better agreement with the McNeice data shown in Figure 7 may be no more than the serendipity associated with the lack of tension stiffening used by MAT1 compensated for by the under integration. The eight-node solid elements with the MAT1 characterization, in Figure 7, shows relatively good representation of the slab stiffness with a slight under-prediction. The ultimate load predicted by this model has merit if the McNeice data are extrapolated. As the ultimate load is approached, most of the integration points below the neutral axis are cracked, and the ultimate load predicted by the MAT1 constitutive model should be reasonably close to the experimental value.

CONCLUSION

Both the MAT1 and MAT2 constitutive models have shown the capability to provide solutions that characterize structures loaded beyond their design basis. Comparisons to the McNeice data provide confidence in their capability to produce accurate predictions. While both constitutive models provide adequate stability with well integrated shell elements, MAT1 provides for slightly better solution stability with the use of solid elements. Whenever possible, it is best to create the mesh so that elements that experience significant tension contain reinforcement. The MAT2 constitutive model allows for greater flexibility in specifying both the yield surface and tensile behavior than MAT1. Some of these

parameters, such as tension stiffening, are not usually known without testing. In the absence of test data, confidence in the solution can be gained by using two independent constitutive models. The ABAQUS finite-element program in conjunction with UMAT90 makes this a relatively simple procedure because the same finite-element model can be used.

When used in dynamic analyses, UMAT90 has several features that could allow for a better representation of the reinforced concrete than the ABAQUS constitutive model. These features include a concrete material property database accessed by specifying the ultimate compressive strength, damping associated with open and closed cracks on an element integration point basis, and reduction of the elastic stiffness associated with inelastic compressive strains for cyclic loading. UMAT90 has been used extensively in static ultimate load analyses such as the pre- and post-test analyses of the Sandia 1:6 scale reinforced-concrete containment model pressurized to failure (Clauss 1987; Clauss 1989). Its use with ABAQUS in dynamic analyses is still rather novel. Prudence would suggest an independent constitutive model be used as verification. The ABAQUS constitutive model post-cracking behavior does not include degradation of the concrete Young's modulus, hence the ABAQUS constitutive model performs best with relatively monotonic loads (HKS 1989a).

The standard solution procedure used with MAT1 includes the use of the NOSTOP option, which allows the solution to continue beyond the point where the maximum specified iterations fail to satisfy the equilibrium convergence criteria. This approach requires the analyst to judge the appropriateness of the solution. In addition, the automatic time step optimization in ABAQUS is circumvented with the NOSTOP option. Unlike the Riks algorithm, however, the standard solution procedure allows restart capability.

ANTICIPATED DEVELOPMENTS

The developers of ABAQUS and ANACAP-U are continually upgrading the reinforced-concrete constitutive models. It is expected that with the next release of ABAQUS, a new fracture-mechanics-based, smeared-crack model will be available. This new model is designed to be mesh independent, so that tension stiffening can be specified in a consistent manner. It is also expected that the NOSTOP option will be available for use in dynamic analyses as it is currently for use in static analyses. The next release of UMAT90 is expected to include a modified 'rough crack' model that accounts for reinforcement density and aggregate size. It also promises to provide more numerical stability.

REFERENCES

ANATECH Research Corporation, 1990a, *ANACAP-U User's Manual and Theory Report*, Vol. 1 and 2, Version 90-1.0, San Diego, California.

ANATECH Research Corporation, 1990b, *ANACAP-U Verification Manual*, Version 90-1.0, San Diego, California.

Clauss, D. B., 1987, "Round-Robin Pretest Analyses of a 1:6-Scale Reinforced Concrete Containment Model Subject to Static Internal Pressurization," NUREG/CR-4913, SAND87-0891, Sandia National Laboratories, Albuquerque, New Mexico.

Clauss, D. B., 1989, "Round-Robin Analyses of the Behavior of a 1:6-Scale Reinforced Concrete Containment Model Pressurized to Failure: Posttest Evaluations," NUREG/CR-5341, SAND89-0349, Sandia National Laboratories, Albuquerque, New Mexico.

Cope, R. J., 1984, "Material Modeling of Real Reinforced Concrete Slabs," *Proceedings of the International Conference of Computer-Aided Analysis and Design of Concrete Structures Part I.*

Cristfield, M. A., 1984," Difficulties with Current Numerical Models for Reinforced Concrete and Some Tentative Solutions," *Computer Aided Analysis and of Design Concrete Structures Part I.*

Cristfield, M. A., 1986, "Snap-Through and Snap-Back Response in Concrete Structures and the Dangers of Under Integration," *International Journal for Numerical Methods in Engineering*, Vol. 22, pp 751-767.

Gilbert, R. I., and Warner, R. F., 1978, "Tension Stiffening in Reinforced Concrete Slabs," *Journal of the Structural Division*, ASCE, No. ST12, Paper 14211, pp. 1885-1900.

Gonzalez-Vidosa, F., et al., 1986, "On the Numerical Instabilities of the Smeared Crack Approach in the Nonlinear Modeling of Concrete Structures," *Communications in Applied Numerical Methods.*

HKS, 1989a, *ABAQUS Theoretical Manual*, Version 4.8, Hibbitt, Karlsson & Sorensen, Inc., Providence, Rhode Island.

Jofriet, J. C., and McNeice, G. M., 1971, "Finite Element Analysis of Reinforced Concrete Slabs," *Journal of the Structural Division*, ASCE, Vol. 97, No. ST3, Proc. Paper 7963, pp. 785-906.

Schnobrich, W. C., 1990, "The Role of Finite Element Analysis of Reinforced Concrete Structures," *Analysis of Concrete Structures ASCE*, 1990.

Table 1. Analysis Parameter Matrix Summary.

Case number	Solution technique	Concrete material	Steel material	Liner	Large disp.	Element type	Integration points	Maximum deflection cm (in.)
1	Riks[a]	MAT2[b]	EPP[c]	No	No	Shell	2x2x9	38.10 (15.0)
2	NOSTOP[d]	MAT2	EPP	No	No	Shell	2x2x9	1.06 (0.42)
3	Riks	MAT2	EPP	No	Yes	Shell	2x2x9	6.10 (2.4)
4	Riks	MAT2	TE[e]	No	No	Shell	2x2x9	6.60 (2.6)
5	Riks	MAT2/SH[f]	EPP	No	No	Shell	2x2x9	241.3 (95.0)
6	Riks	MAT2	EPSH[g]	No	No	Shell	2x2x9	12.45 (4.9)
7	Riks	MAT2	EPP	Yes	No	Shell	2x2x9	8.13 (3.2)
8	NOSTOP	MAT2	EPP	Yes	No	Shell	2x2x9	8.13 (3.2)
9	NOSTOP	MAT1[h]	EPP	No	No	Shell	2x2x9	22.86 (9.0)
10	NOSTOP	MAT1	TE	No	No	Shell	2x2x9	>254.0 (100.0)
11	NOSTOP	MAT1	EPP	Yes	No	Shell	2x2x9	>254.0 (100.0)
12	NOSTOP	MAT1	EPP	No	Yes	Shell	2x2x9	31.75 (12.5)
13	Riks	MAT2	EPP	No	No	Shell	2x2x3	2.54 (1.0)
14	Riks	MAT2	EPP	No	No	Solid	2x2x2	0.08 (0.03)
15	NOSTOP	MAT2	EPP	No	No	Solid	2x2x2	0.46 (0.18)
16	NOSTOP	MAT1	EPP	No	No	Shell	2x2x3	30.48 (12.0)
17	NOSTOP	MAT1	EPP	No	No	Solid	2x2x2	1.35 (0.53)

[a]Riks = Modified Riks solution algorithm.
[b]MAT2 = ABAQUS concrete constitutive model.
[c]EPP = Elastic perfectly plastic.
[d]NOSTOP = Deactivates equilibrium convergence criteria.
[e]TE = Totally elastic.
[f]/SH = With strain hardening.
[g]EPSH = Elastic-plastic strain hardening.
[h]MAT1 = UMAT90 concrete constitutive model.

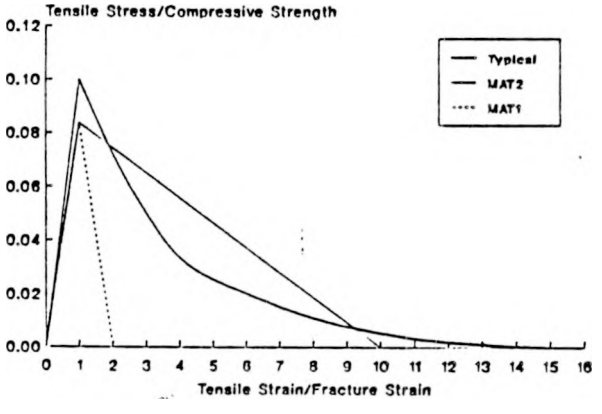

Fig. 1 Reinforced concrete tensile stress vs strain diagram

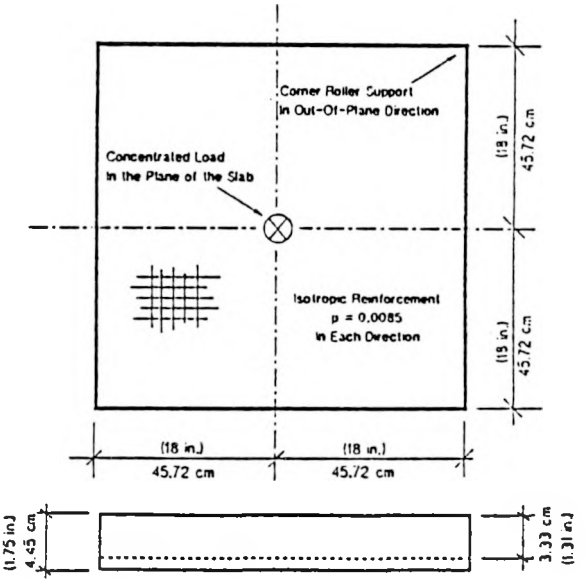

Fig. 2 McNeice slab layout

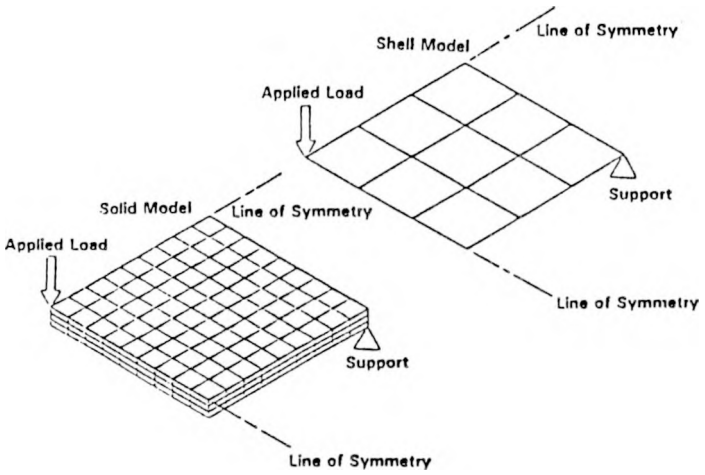

Fig. 3 Finite-element mesh

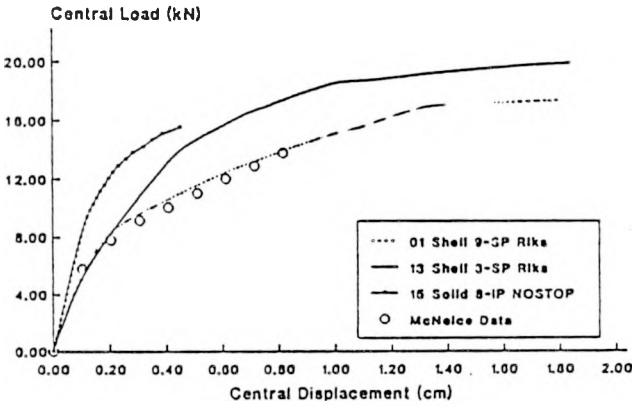

Fig. 6 McNeice slab ABAQUS element/integration point accuracy comparison

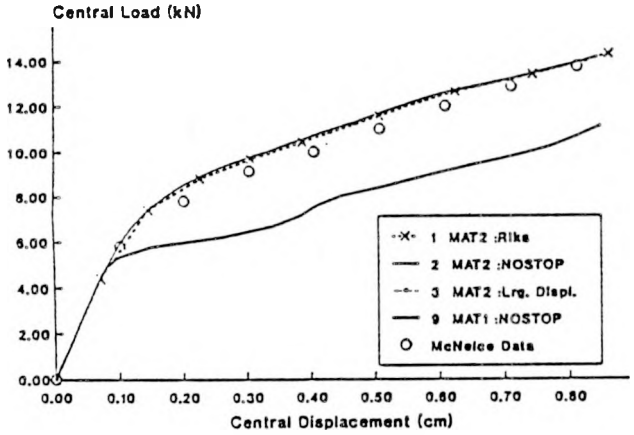

Fig. 4 McNeice slab solution accuracy comparison

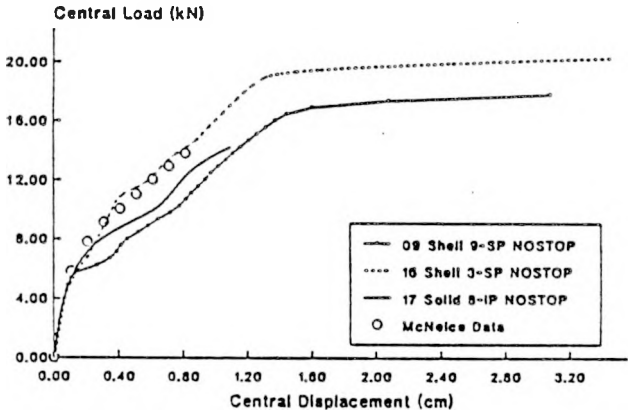

Fig. 7 McNeice slab UMAT90 element/integration point accuracy comparison

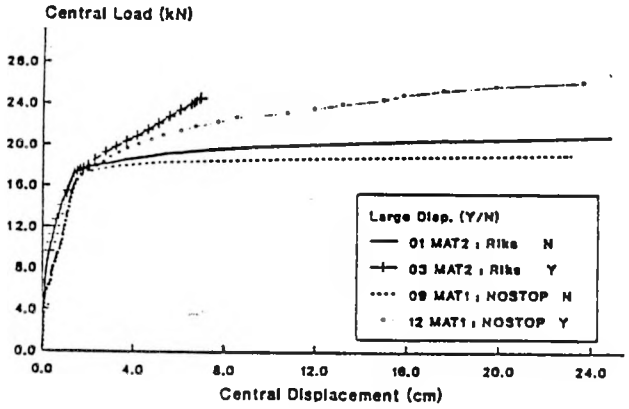

Fig. 5 McNeice slab large displacement theory trend comparison

DISTRIBUTION

Number of copies

OFFSITE

1 American Society of Mechanical Engineers
345 E. 47th Street
New York, New York 10017

ONSITE

6 U.S. Department of Energy-
Richland Operations Office

R. F. Christensen (5)	R4-04
Public Reading Room	A1-65

17 Westinghouse Hanford Company

W. W. Chen	H5-57
T. J. Conrads	H5-53
A. D. Dyrness (2)	H5-56
G. L. Fox	L5-07
D. J. Green	S5-75
J. L. Julyk	L5-56
M. R. Lindquist	H5-57C
C. J. Moore	H5-56
R. B. Pan	H5-56
L. K. Severud	H5-60
J. Sprouse	L8-07
J. B. Truitt	H5-56
E. O. Weiner	H5-53
Document Clearance	L8-07
Document Processing and Distribution (2)	L8-15